Compared Performance of High-Sensitivity Cameras Dedicated to Myocardial Perfusion SPECT: A Comprehensive Analysis of Phantom and Human Images

Laetitia Imbert[1–4], Sylvain Poussier[3,5], Philippe R. Franken[6], Bernard Songy[7], Antoine Verger[3–5], Olivier Morel[4], Didier Wolf[1], Alain Noel[1], Gilles Karcher[3–5], and Pierre-Yves Marie[3,4,8]

[1]CRAN–UMR 7039, Université de Lorraine–CNRS, Vandoeuvre, France; [2]Department of Radiotherapy, Centre Alexis Vautrin, Vandoeuvre, France; [3]Nancyclotep Experimental Imaging Platform, Nancy, France; [4]Department of Nuclear Medicine, CHU–Nancy, Nancy, France; [5]INSERM, U947, Nancy, France; [6]Department of Nuclear Medicine, Centre Antoine Lacassagne, Nice, France; [7]Department of Nuclear Medicine, Centre Cardiologique du Nord, Saint-Denis, France; and [8]INSERM, U961, Nancy, France

Differences in the performance of cadmium-zinc-telluride (CZT) cameras or collimation systems that have recently been commercialized for myocardial SPECT remain unclear. In the present study, the performance of 3 of these systems was compared by a comprehensive analysis of phantom and human SPECT images. **Methods:** We evaluated the Discovery NM 530c and DSPECT CZT cameras, as well as the Symbia Anger camera equipped with an astigmatic (IQ·SPECT) or parallel-hole (conventional SPECT) collimator. Physical performance was compared on reconstructed SPECT images from a phantom and from comparable groups of healthy subjects. **Results:** Classifications were as follows, in order of performance. For count sensitivity on cardiac phantom images (counts·s^{-1}·MBq^{-1}), DSPECT had a sensitivity of 850; Discovery NM 530c, 460; IQ·SPECT, 390; and conventional SPECT, 130. This classification was similar to that of myocardial counts normalized to injected activities from human images (respective mean values, in counts·s^{-1}·MBq^{-1}: 11.4 ± 2.6, 5.6 ± 1.4, 2.7 ± 0.7, and 0.6 ± 0.1). For central spatial resolution: Discovery NM 530c was 6.7 mm; DSPECT, 8.6 mm; IQ·SPECT, 15.0 mm; and conventional SPECT, 15.3 mm, also in accordance with the analysis of the sharpness of myocardial contours on human images (in cm^{-1}: 1.02 ± 0.17, 0.92 ± 0.11, 0.64 ± 0.12, and 0.65 ± 0.06, respectively). For contrast-to-noise ratio on the phantom: Discovery NM 530c had a ratio of 4.6; DSPECT, 4.1; IQ·SPECT, 3.9; and conventional SPECT, 3.5, similar to ratios documented on human images (5.2 ± 1.0, 4.5 ± 0.5, 3.9 ± 0.6, and 3.4 ± 0.3, respectively). **Conclusion:** The performance of CZT cameras is dramatically higher than that of Anger cameras, even for human SPECT images. However, CZT cameras differ in that spatial resolution and contrast-to-noise ratio are better with the Discovery NM 530c, whereas count sensitivity is markedly higher with the DSPECT.

Key Words: CZT-cameras; high-speed SPECT; myocardial perfusion imaging; count sensitivity

J Nucl Med 2012; 53:1897–1903
DOI: 10.2967/jnumed.112.107417

Stress myocardial SPECT has been markedly enhanced by the recent commercialization of cameras with semiconductor (cadmium-zinc-telluride [CZT]) detectors or new collimation systems. These improved systems enhance the sensitivity of count detection and thereby enable recording times or tracer doses to be reduced, a property that has highly favorable consequences on patient comfort and radiation exposure (*1–4*). This enhancement is based mainly on acquisitions that are heart-centric but obtained with very different technologies: first, for the IQ·SPECT system (Siemens Medical Solutions (*5–8*)), an Anger camera equipped with collimators convergent on the image center (astigmatic collimators); second, for the DSPECT system (Spectrum Dynamics (*9–13*)), mobile columns of CZT detectors with wide parallel-hole collimators; and third, for the Discovery NM 530c system (GE Healthcare (*14–21*)), fixed CZT detectors with multipinhole collimators.

The respective performance of these new cameras and collimation systems has been analyzed, but only separately (*6,11,14*). To our knowledge, there has been no direct head-to-head comparison of the performance of the IQ·SPECT, DSPECT, and Discovery NM 530c systems. In addition, their performance was never compared for human SPECT images and, thus, with the additional confusing influence of breathing and cardiac motion, along with body attenuation and diffusion.

This study directly compared the performance of IQ·SPECT, DSPECT, and Discovery NM 530c in routine conditions of SPECT recording and reconstruction and by a comprehensive analysis of SPECT images from phantoms and from healthy subjects.

Received Apr. 18, 2012; revision accepted Jul. 17, 2012.
For correspondence contact: Laetitia Imbert, Médecine Nucléaire, Hôpital de Brabois, CHU-Nancy, Allée du Morvan, 54500 Vandoeuvre-lès-Nancy, France.
E-mail: l.imbert@nancy.unicancer.fr
Published online Nov. 8, 2012.

TABLE 1
Parameters Commonly Used for SPECT Recording and Reconstruction

Parameter	Discovery NM 530c	DSPECT	IQ·SPECT	Conventional SPECT
Recording				
Collimator	Multipinhole	Wide-angle parallel hole	Astigmatic	LEHR or parallel hole
Energy window	140 keV ± 10%	140 keV ± 10%	140 keV ± 7.5%	140 keV ± 7.5%
Number of projections	19	120 (×9 blocks)	17 (×2 heads)	16 (×2 heads)
Detector angle between consecutive projections	None (fixed detector)	0.4°–7°*	6°	3°
Reconstruction				
Method	Iterative 3D	Iterative 3D	Iterative 3D	Iterative 3D
Number of iterations	60	7	10	8
Number of subsets	1	32	3	4
Interiteration filter	—	Kernel (0.125)	—	—
Final filter	Butterworth (order, 7; cutoff, 0.37 cm^{-1})	Normalizing filter†	Gaussian (10 mm FWHM)	Gaussian (10 mm FWHM)
Pixel size (mm)	4.0	4.92	4.8	6.6

*Angles are approximately 0.4° for projections passing through cardiac region (as defined by adjusted region of interest on prescan images) and up to 7° for other projections.
†Way in which normalizing filter works is proprietary information of Spectrum Dynamics.
LEHR = low-energy high-resolution; 3D = 3-dimensional; FWHM = full width at half maximum.

MATERIALS AND METHODS

γ-Cameras and Collimation Systems

Table 1 summarizes the conventional recording and reconstruction parameters that were used for the 4 cameras.

The DSPECT camera was analyzed at the University Hospital of Nancy. As previously described (*9–11*), this camera operates with 9 mobile blocks of pixelated CZT detectors (pixel size, 2.5 × 2.5 mm) associated with a wide-angle square-hole tungsten collimator. A total of 120 projections are recorded by each block by means of a region-centric acquisition that maximizes counts emanating from the heart area, which was previously defined on a short prescan acquisition. A specific algorithm of iterative reconstruction is used to compensate for the collimator-related loss in spatial resolution (*9–11*). All the reconstruction parameters currently recommended for clinical routine (Table 1) were used, except for the cardiac anatomic model of the DSPECT camera, which constrains the shape and thickness of left ventricular walls (*12*).

The Discovery NM 530c camera was analyzed at the North Cardiology Centre in Saint-Denis, France. This camera operates with 19 fixed detectors, which are placed over an arc of 180° and orientated to focus on the heart area (*15,16*). Each detector involves 4 modules of 32 × 32 CZT pixels (pixel size, 2.5 × 2.5 mm) and is associated with a tungsten pinhole collimator with an effective aperture of 5.1 mm (*19,20*). Nineteen projections are thus recorded, and an iterative reconstruction allows modeling for collimator geometry.

The Symbia camera (Siemens Medical Solutions) is a dual-head Anger camera for which cardiac imaging can be performed either with a low-energy high-resolution collimator (for conventional SPECT) or with a high-sensitivity astigmatic collimator involving a convergent geometry for the image center and parallel holes for the edges (for IQ·SPECT) (*6*). Conventional SPECT and IQ·SPECT were assessed in the University Hospitals of Nice and Nancy, respectively. For conventional SPECT, the detectors were placed close to the patient in a body-contour mode, whereas for IQ·SPECT, rotation of the detectors was circular with a 28-cm radius and centered on the heart (*12*). SPECT images are routinely reconstructed with 3-dimensional iterative algorithms (*22*) and with an additional correction for the geometry of the astigmatic collimator for IQ·SPECT (*23,24*).

Selection of Human SPECT Images

Presumably healthy male subjects were retrospectively selected for 4 groups, up to a total of 12 in each group, if they fulfilled the following criteria: first, had been routinely referred for exercise myocardial SPECT with ^{99m}Tc-sestamibi on the Discovery NM 530c (first group in Saint-Denis), the DSPECT (second group in Nancy), or the Symbia equipped for IQ·SPECT (third group in Nancy) or conventional SPECT (fourth group in Nice); second, were between 50 and 70 y old; third, weighed less than 100 kg; fourth, had no history of coronary artery disease and less than a 10% pretest likelihood of coronary artery disease, according to the Diamond and Forester tables; fifth, had achieved maximal exercise on testing (≥85% of predicted maximal heart rate (220 − age)); and finally, had exercise test results and SPECT images that were considered normal by experienced observers. Images were rendered anonymous, and no approval of any ethical committee was required for this retrospective analysis of routinely recorded human SPECT images.

Phantom SPECT Images

A commercially available phantom mimicking the shape of a normal heart was used (cardiac insert; Biodex Medical Systems) (Fig. 1). The left ventricular cavity was filled with water, and the left ventricular walls were filled with a solution containing only 10 MBq of ^{99m}Tc to avoid any saturation-related loss in counts. This phantom was placed at the center of the field of view and orientated in 45° left-anterior and 45° caudal directions. SPECT images were obtained using the parameters listed in Table 1. Time per projection was modulated to obtain a total recorded activity of approximately 500 kilocounts.

Performance Parameters

The selection of 3 major performance parameters—tomographic count sensitivity, spatial resolution, and contrast-to-noise ratio—was based on their ability to be determined on phantoms and to be assessed at least indirectly on human SPECT images.

Tomographic Count Sensitivity. Tomographic count sensitivity was measured on the reconstructed SPECT images of the phantom. The total number of recorded counts was determined with a manually adjusted elliptic region of interest, and count sensitivity was calculated using the following formula:

$$\text{Total recording counts}/[\text{recording time (s)} \times \text{left ventricular activity (MBq)}].$$

This count sensitivity could not be directly determined for the human SPECT images. The actual left ventricular activities were unknown and thus replaced in the formula by the activities that were injected intravenously at peak exercise. Thereby, intergroup comparisons were made with the myocardial counts normalized to recording times (s) and injected activities (MBq). However, it is likely that these comparisons were dependent mainly on the differences in count sensitivity between the 4 camera groups. These groups were indeed constituted in such a way as to standardize factors that can affect cardiac uptake of tracer (exclusion of subjects with submaximal testing) or that clearly change the conditions of body attenuation and diffusion (inclusion of male-only subjects weighing < 100 kg).

The measurements were corrected for decay, and further corrections were needed for the conventional SPECT protocol in which exercise SPECT was performed after rest SPECT. Myocardial activity, corresponding to exercise-only injection, was then obtained after subtraction of residual myocardial activity from rest injection. This residual activity was obtained with the myocardial activity that was measured on the previous rest SPECT (in counts·s^{-1}) and corrected for decay.

Reconstructed Spatial Resolution. Reconstructed spatial resolution was determined according to the National Electrical Manufacturers Association NU-1 2001 protocol, with the exception that the reconstruction SPECT parameters were those recommended for clinical routine (Table 1). SPECT images were obtained from an insert with 3 linear sources of 1.5-mm internal diameter. These sources were filled with a 2 MBq/mL solution of ^{99m}Tc and placed in the longitudinal direction. Horizontal and vertical profiles were generated for each line source on a median axial reconstructed slice. Central, tangential, and radial resolutions were determined with the open-source AMIDE software as the full width at half maximum of gaussian fit (*19*).

Spatial resolution could not be directly measured on human SPECT images but could be estimated through a quantitative sharpness profile, a parameter that is dramatically influenced by spatial resolution (*25–27*). As illustrated in Figure 2, a sharpness index was determined on the horizontal profile of the midventricular short-axis slice. This index was computed as the maximal slope of the decrease in myocardial counts (cm^{-1}) on the epicardial border of the lateral wall and after exclusion of the low-count part of the profile (activities $< 25\%$ of the maximal value).

Contrast-to-Noise Ratio. Contrast-to-noise ratio reflects the ability to generate an image contrast that may not be due to noise fluctuations yet is clinically useful (*28,29*). This ratio was determined on the midventricular short-axis slice of each SPECT recording (Fig. 1). Mean myocardial counts and corresponding SD were determined on a ring-shaped region of interest encompassing the endocardial and epicardial borders. Mean background counts and corresponding SD were determined on a half-moon–shaped region of interest, at 15 mm from the lateral wall. Contrast-to-noise ratio was estimated with the following formula:

$$\left(M_{My} - M_{BG}\right) \Big/ \sqrt{\left[SD_{My}\right]^2 + \left[SD_{BG}\right]^2},$$

where M_{My} is mean myocardial counts, M_{BG} is mean background counts, SD_{My} is mean myocardial SD, and SD_{BG} is mean background SD.

RESULTS

Characteristics of the Study Groups

Four groups of 12 presumably healthy subjects, corresponding to each of the 4 cameras, were created. As detailed in Table 2, age, body weight, and maximal heart rate at exercise were comparable in all 4 groups.

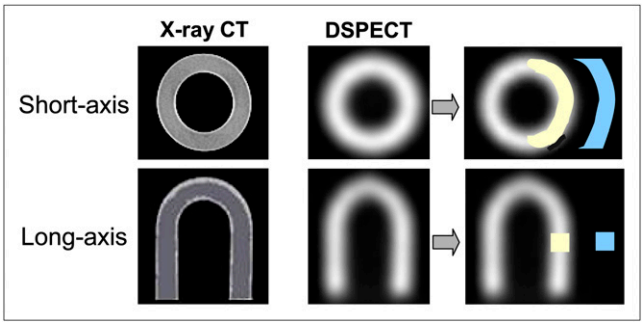

FIGURE 1. Images of cardiac phantom provided by CT and by DSPECT camera, as well as representation of background (blue) and myocardial (yellow) regions of interest, which were used for determining contrast-to-noise ratio.

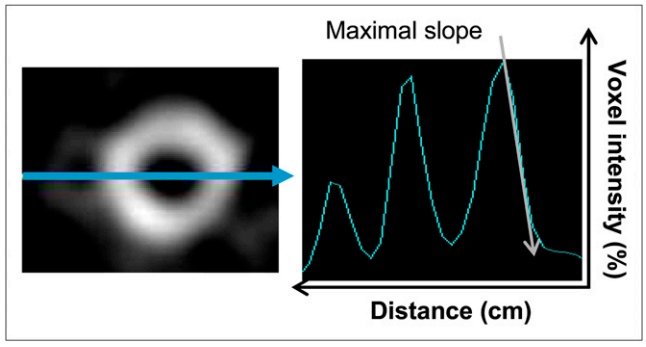

FIGURE 2. Example, on median short-axis slice, of determination of maximal slope of epicardial border of left lateral wall, representing sharpness index. Distance is expressed in centimeters, and voxel intensity is expressed in percentage of maximal myocardial voxel value.

TABLE 2
Main Characteristics of the 4 Camera Groups Involved in Clinical Study

Characteristic	Discovery NM 530c	DSPECT	IQ·SPECT	Conventional SPECT
Number of subjects	12	12	12	12
Age (y)	53 ± 10	56 ± 10	53 ± 8	57 ± 7
Body weight (kg)	80 ± 10	80 ± 7	84 ± 13	83 ± 13
Study protocol	1-d stress–rest	1-d stress–rest	1-d stress–rest	1-d rest–stress
Tracer	Sestamibi	Sestamibi	Sestamibi	Sestamibi
Activity injected at exercise (MBq)*	132 ± 22	168 ± 62	318 ± 34	1,073 ± 177
Maximal heart rate at exercise (%†)	93 ± 8	95 ± 4	91 ± 7	91 ± 4
Recording time (min)	10	6	4.5	16
Patient position	Prone	Semireclining	Prone	Supine
Total myocardial counts ($\times 10^3$)	447 ± 96	625 ± 198	214 ± 60	1,019 ± 190

*Corrected for physical decay at half-time of SPECT recording.
†Expressed in percentage of maximal predicted value (220 – age).

However, there were substantial differences in the conditions under which SPECT was recorded, especially with regard to patient position (prone for IQ·SPECT and Discovery NM 530c, supine for conventional SPECT, and semireclining on a dedicated chair for DSPECT (*9*)), the 1-d study protocols (starting with rest SPECT for the conventional SPECT group and with exercise SPECT for the other groups), and the injected activities and recording times (Table 2). Therefore, the total myocardial counts were different in the 4 groups. The lowest values were in the IQ·SPECT group, and the highest values were in the conventional SPECT group (Table 2).

Performance Parameters

Tomographic count sensitivities were determined with the phantom for total recording counts, which were near or slightly higher than 500 kilocounts for conventional SPECT (578 kilocounts), IQ·SPECT (581 kilocounts), DSPECT (580 kilocounts), and Discovery NM 530c (497 kilocounts). As illustrated in Figure 3, this count sensitivity was 130 counts·s^{-1}·MBq^{-1} with conventional SPECT and was improved 3-fold with IQ·SPECT (390 counts·s^{-1}·MBq^{-1}), about 4-fold with Discovery NM 530c (460 counts·s^{-1}·MBq^{-1}), and nearly 7-fold with DSPECT (850 counts·s^{-1}·MBq^{-1}).

Concordant results were also achieved for myocardial counts normalized to injected activities from human examinations (in counts·s^{-1}·MBq^{-1}: conventional SPECT, 0.6 ± 0.1; IQ·SPECT, 2.7 ± 0.7; Discovery NM 530c, 5.6 ± 1.4; and DSPECT, 11.4 ± 2.6) (Fig. 3).

The best spatial resolution was achieved with the Discovery NM 530c (6.7 mm for central spatial resolution, Fig. 3). Documented values were higher for the DSPECT (8.6 mm for central spatial resolution) and higher still for IQ·SPECT (15.0 mm) and conventional SPECT (15.3 mm). In addition, a concordant classification was obtained for the sharpness index of myocardial contours on human images (in cm^{-1}: Discovery NM 530c, 1.02 ± 0.17; DSPECT, 0.92 ± 0.11; IQ·SPECT, 0.64 ± 0.12; and conventional SPECT, 0.65 ± 0.06) (Fig. 3).

Figure 4 displays representative SPECT images obtained with the 4 cameras for human images from our study population and for the phantom after simulation of a small parietal defect (insertion of a small solid cube 15 mm in length).

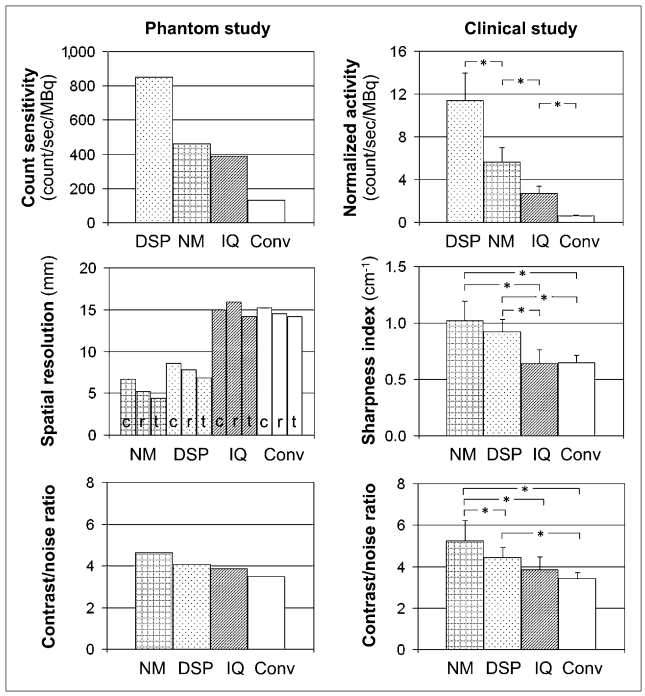

FIGURE 3. Comparison of the 4 cameras. Count sensitivity was determined for phantom (top left) and indirectly assessed for human (top right) SPECT images by normalizing counts to recording time and injected activity. Spatial resolution was determined for phantom insert (middle left) and indirectly assessed for human (middle right) SPECT images using sharpness index for myocardial contours. Contrast-to-noise ratio was determined for phantom (bottom left) and human (bottom right) SPECT images. Conv = conventional SPECT; DSP = DSPECT; IQ = IQ·SPECT; NM = Discovery NM 530c; c = central resolution; r = radial resolution; t = tangential resolution.

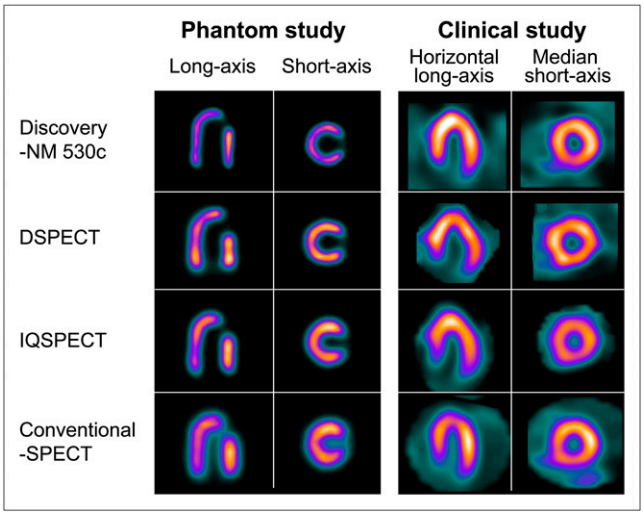

FIGURE 4. Representative SPECT images obtained with 4 different cameras: with phantom after simulation of small parietal defect (insertion of small solid cube 15 mm in length) (left) and in subjects involved in clinical part of study (right).

The contrast-to-noise ratios obtained for the phantom (Fig. 3) were higher for Discovery NM 530c (4.6) and lower for DSPECT (4.1), IQ·SPECT (3.9), and conventional SPECT (3.5). In addition, an equivalent order of classification was documented for human images: 5.2 ± 1.0 for Discovery NM 530c, 4.5 ± 0.5 for DSPECT, 3.9 ± 0.6 for IQ·SPECT, and 3.4 ± 0.3 for conventional SPECT (Fig. 3).

DISCUSSION

Objective measurements reflecting performance have already been described for the Discovery NM 530c and DSPECT cameras, as well as for the IQ·SPECT collimation system (*6,11,14*). However, the differences in count sensitivity, as well as in image quality, remain unclear, especially in routine patient SPECT.

In the present study, head-to-head comparisons were conducted by analyzing global performance parameters that could be at least indirectly assessed on human SPECT images, that is, count sensitivity, spatial resolution, and contrast-to-noise ratio. Tomographic count sensitivities were determined on a cardiac phantom rather than on point sources to better reflect the conditions of routine SPECT. These count sensitivities were nevertheless close to those previously published for point sources placed at the center of the field of view (Discovery NM 530c (*20*), DSPECT (*11*), IQ·SPECT (*12*)). Of greater significance is the fact that head-to-head comparisons gave evidence of a dramatic superiority for the DSPECT camera. The count sensitivity provided by this camera was indeed around 7-fold higher than that from conventional SPECT and nearly 2-fold higher than those from Discovery NM 350c and from IQ·SPECT.

However, these differences could not be directly extrapolated to the conditions for human SPECT because of several interfering factors such as breathing and cardiac motion, as well as body attenuation and diffusion. Hence, tomographic count sensitivity was also indirectly assessed on human SPECT images. For this purpose, myocardial counts normalized to recording times and injected activities were compared among groups of presumably healthy subjects (low pretest likelihoods and normal test results) who had undergone exercise SPECT on each of the 4 cameras and who had comparable characteristics (exclusion of subjects with submaximal testing, inclusion of male-only subjects weighing < 100 kg).

The normalized myocardial activities thus obtained represented approximately 1% of the count sensitivities obtained on the cardiac phantom. This low percentage can be explained by several factors: that only about 5% of the injected activity is likely to pass through coronary vessels (coronary flow expressed as percentage of cardiac flow) (*30*), that less than 40% of this amount will be retained within the myocardial tissue (retention fractions of sestamibi under high-flow conditions (*31,32*)), and that the addition of body attenuation further decreases the number of detected photons.

Finally, the results provided by these normalized activities were highly coherent with the count sensitivities from the phantom—in particular, 2-fold higher values for DSPECT than for Discovery NM 530c—possibly because of the differences in collimation systems between the Discovery NM 530c (pinholes) and the DSPECT (wide parallel holes). In addition, the heart-centric methods of collimation for these 2 CZT cameras are likely to explain most of their enhanced count sensitivity, when compared with conventional SPECT (*11,13,14*).

Spatial resolution was analyzed with a National Electrical Manufacturers Association–defined insert but with routine reconstruction parameters and, thus, in a different manner from that recommended in the National Electrical Manufacturers Association procedures (large voxel size, iterative methods of reconstruction). Therefore, our values of full width at half maximum were not the same as those already published (*11,14*) but were nevertheless highly coherent while showing much better results with CZT cameras and especially with the Discovery NM 530c. Furthermore, equivalent differences were observed with regard to the sharpness of the myocardial contours from human images (Fig. 3), a parameter strongly linked to spatial resolution (*25,26,33*). This finding provides evidence that the improvement in spatial resolution from CZT cameras has a true impact on patients' SPECT images.

These differences in spatial resolution among the 4 cameras also correlated with corresponding differences in contrast-to-noise ratio (Fig. 3). This observation illustrates the general consideration that the contrast of myocardial SPECT images depends mainly on the level of reconstructed resolution. In addition, the difference in collimation systems herein is also a likely explanation for much of

the difference in spatial resolution and contrast between the Discovery NM 530c (pinholes) and the DSPECT (wide parallel holes). However, it is the pixelated organization of CZT detectors that is the most likely explanation of the enhancement in spatial resolution and contrast between CZT and Anger SPECT (*13,14*).

As a function of reconstruction parameters, there is a balance between reconstructed noise on the one hand and contrast and spatial resolution on the other. Our analyses were performed with routine reconstruction parameters and, thus, at a balance level that is considered to be well adapted to clinical routine. However, the choice of other reconstruction parameters could have affected our results. In particular, it is likely that the image quality parameters of the CZT cameras could have been enhanced using smaller energy windows, with only a limited loss in count sensitivity, but further studies are required to determine the optimal energy windows for CZT SPECT. Additional enhancements might be achieved using cardiac models, such as that available and recommended for the DSPECT camera; by new low-dose protocols (*34*); and by triggering breathing, especially when using the stationery detectors of the Discovery NM 530c (*17*).

As recommended by the manufacturers, thresholds of ±10% were applied for the ^{99m}Tc energy windows of the DSPECT and Discovery NM 530c cameras as opposed to ±7.5% for the Symbia Anger camera. However, this difference is unlikely to have any significant impact on our results, particularly for the recording counts, which increase no more than 10% when a ±10% energy window is used on the Symbia camera instead of a ±7.5% window.

In addition, human SPECT images were analyzed here only in small subgroups of highly selected healthy subjects. Therefore, it is likely that the further analysis of larger groups with more varied characteristics would be informative.

CONCLUSION

By a comprehensive analysis of phantom and human SPECT images, this study provided evidence that the physical performance of CZT cameras is dramatically higher than that of Anger cameras, even when equipped with astigmatic collimators. However, the 2 CZT cameras are inherently different; spatial resolution and contrast-to-noise ratio are better with the Discovery NM 530c, whereas detection sensitivity is markedly higher with the DSPECT.

DISCLOSURE STATEMENT

The costs of publication of this article were defrayed in part by the payment of page charges. Therefore, and solely to indicate this fact, this article is hereby marked "advertisement" in accordance with 18 USC section 1734. No other potential conflict of interest relevant to this article was reported.

ACKNOWLEDGMENTS

We thank the Nancy University Hospital for organizational support, the French Research Ministry for financial support (a 2009 grant from CIFRE), and the staffs of General Electric France, Siemens France, and Spectrum Dynamics for technical support.

REFERENCES

1. Schillaci O, Danieli R. Dedicated cardiac cameras: a new option for nuclear myocardial perfusion imaging. *Eur J Nucl Med Mol Imaging.* 2010;37:1706–1709.
2. Mouden M, Timmer JR, Ottervanger JP, et al. Impact of a new ultrafast CZT SPECT camera for myocardial perfusion imaging: fewer equivocal results and lower radiation dose. *Eur J Nucl Med Mol Imaging.* 2012;39:1048–1055.
3. Duvall WL, Croft LB, Ginsberg ES, et al. Reduced isotope dose and imaging time with a high-efficiency CZT SPECT camera. *J Nucl Cardiol.* 2011;18:847–857.
4. Songy B, Guernou M, Lussato D, et al. Low-dose thallium-201 protocol with a cadmium-zinc-telluride cardiac camera. *Nucl Med Commun.* 2012;33:464–469.
5. Hawman PC, Haines EJ. The cardiofocal collimator: a variable focus collimator for cardiac SPECT. *Phys Med Biol.* 1994;39:439–450.
6. Rajaram R, Bhattacharya M, Ding X, et al. Tomographic performance characteristics of the IQSPECT system. *IEEE Nucl Sci Symp Conf Rec.* 2011; 2451–2456.
7. Garcia EV, Faber TL, Esteves FB. Cardiac dedicated ultrafast SPECT cameras: new designs and clinical implications. *J Nucl Med.* 2011;52: 210–217.
8. Garcia EV, Faber TL. New trends in camera and software technology in nuclear cardiology. *Cardiol Clin.* 2009;27:227–236.
9. Patton JA, Slomka PJ, Germano G, Berman DS. Recent technologic advances in nuclear cardiology. *J Nucl Cardiol.* 2007;14:501–513.
10. Sharir T, Ben-Haim S, Merzon K, et al. High-speed myocardial perfusion imaging initial clinical comparison with conventional dual detector anger camera imaging. *JACC Cardiovasc Imaging.* 2008;1:156–163.
11. Erlandsson K, Kacperski K, Van Gramberg D, Hutton BF. Performance evaluation of D-SPECT: a novel SPECT system for nuclear cardiology. *Phys Med Biol.* 2009;54:2635–2649.
12. Slomka PJ, Patton JA, Berman DS, Germano G. Advances in technical aspects of myocardial perfusion SPECT imaging. *J Nucl Cardiol.* 2009;16:255–276.
13. Gambhir SS, Berman DS, Ziffer J, et al. A novel high-sensitivity rapid-acquisition single-photon cardiac imaging camera. *J Nucl Med.* 2009;50: 635–643.
14. Bocher M, Blevis IM, Tsukerman L, Shrem Y, Kovalski G, Volokh L. A fast cardiac gamma camera with dynamic SPECT capabilities: design, system validation and future potential. *Eur J Nucl Med Mol Imaging.* 2010;37: 1887–1902.
15. Duvall WL, Sweeny JM, Croft LB, et al. Comparison of high efficiency CZT SPECT MPI to coronary. *J Nucl Cardiol.* 2011;18:595–604.
16. Herzog BA, Buechel RR, Katz R, et al. Nuclear myocardial perfusion imaging with a cadmium-zinc-telluride detector technique: optimized protocol for scan time reduction. *J Nucl Med.* 2010;51:46–51.
17. Buechel RR, Pazhenkottil AP, Herzog BA, et al. Real-time breath-hold triggering of myocardial perfusion imaging with a novel cadmium-zinc-telluride detector gamma camera. *Eur J Nucl Med Mol Imaging.* 2010;37: 1903–1908.
18. Pazhenkottil AP, Buechel RR, Herzog BA, et al. Ultrafast assessment of left ventricular dyssynchrony from nuclear myocardial perfusion imaging on a new high-speed gamma camera. *Eur J Nucl Med Mol Imaging.* 2010;37:2086–2092.
19. Buechel RR, Herzog BA, Husmann L, et al. Ultrafast nuclear myocardial perfusion imaging on a new gamma camera with semiconductor detector technique: first clinical validation. *Eur J Nucl Med Mol Imaging.* 2010;37:773–778.
20. Esteves FP, Raggi P, Folks RD, et al. Novel solid-state detector dedicated cardiac camera for fast myocardial perfusion imaging: multicenter comparison with standard dual detector cameras. *J Nucl Cardiol.* 2009;16:927–934.

21. Songy B, Lussato D, Guernou M, et al. Comparison of myocardial perfusion imaging using thallium-201 between a new cadmium-zinc-telluride cardiac camera and a conventional SPECT camera. *Clin Nucl Med.* 2011;36:776–780.
22. Vija AH, Zeintl J, Chapman JT, Hawman EG, Hornegger J. Development of rapid SPECT acquisition protocol for myocardial perfusion imaging. *IEEE Nucl Sci Symp Conf Rec*. 2006;3:1811–1816.
23. Vija H, Hawman EG, Engdahl JC. Analysis of a SPECT OSEM reconstruction method with 3D beam modeling and optional attenuation correction: phantom studies. *IEEE Nucl Sci Symp Conf Rec*. 2003;4:2662–2666.
24. Römer W, Reichel N, Vija HA, et al. Isotropic reconstruction of SPECT data using OSEM3D: correlation with CT. *Acad Radiol.* 2006;13:496–502.
25. Shea SM, Kroeker RM, Deshpande V, et al. Coronary artery imaging: 3D segmented k-space data acquisition with multiple breath-holds and real-time slab following. *J Magn Reson Imaging.* 2001;13:301–307.
26. Larson AC, Kellman P, Arai A, et al. Preliminary investigation of respiratory self-gating for free-breathing segmented cine MRI. *Magn Reson Med.* 2005;53:159–168.
27. Leung AO, Paterson I, Thompson RB. Free-breathing cine MRI. *Magn Reson Med.* 2008;60:709–717.
28. Poussier S, Maskali F, Tran N, et al. ECG-triggered ^{18}F-fluorodeoxyglucose positron emission tomography imaging of the rat heart is dramatically enhanced by acipimox. *Eur J Nucl Med Mol Imaging.* 2010;37:1745–1750.
29. Marie PY, Djaballah W, Franken PR, et al. OSEM reconstruction, associated with temporal Fourier and depth-dependant resolution recovery filtering, enhances results from sestamibi and ^{201}Tl 16-interval gated SPECT. *J Nucl Med.* 2005;46:1789–1795.
30. Carù B, Colombo E, Santoro F, Laporta A, Maslowsky F. Regional flow responses to exercise. *Chest.* 1992;101(suppl):223S–225S.
31. Ayalew A, Marie PY, Menu P, et al. A comparison of the overall first-pass kinetics of thallium-201 and technetium-99m MIBI in normoxic and low-flow ischaemic myocardium. *Eur J Nucl Med.* 2000;27:1632–1640.
32. Ayalew A, Marie PY, Menu P, et al. ^{201}Tl and ^{99m}Tc-MIBI retention in an isolated heart model of low-flow ischemia and stunning: evidence of negligible impact of myocyte metabolism on tracer kinetics. *J Nucl Med.* 2002;43:566–574.
33. Groves EM, Bireley W, Dill K, Carroll TJ, Carr JC. Quantitative analysis of ECG-gated high-resolution contrast-enhanced MR angiography of the thoracic aorta. *AJR.* 2007;188:522–528.
34. Nkoulou R, Pazhenkottil AP, Kuest SM, et al. Semiconductor detectors allow low-dose-low-dose 1-day SPECT myocardial perfusion imaging. *J Nucl Med.* 2011;52:1204–1209.

The Journal of NUCLEAR MEDICINE

Compared Performance of High-Sensitivity Cameras Dedicated to Myocardial Perfusion SPECT: A Comprehensive Analysis of Phantom and Human Images

Laetitia Imbert, Sylvain Poussier, Philippe R. Franken, Bernard Songy, Antoine Verger, Olivier Morel, Didier Wolf, Alain Noel, Gilles Karcher and Pierre-Yves Marie

J Nucl Med. 2012;53:1897-1903.
Published online: November 8, 2012.
Doi: 10.2967/jnumed.112.107417

The Journal of Nuclear Medicine is published monthly.
SNMMI | Society of Nuclear Medicine and Molecular Imaging
1850 Samuel Morse Drive, Reston, VA 20190.
(Print ISSN: 0161-5505, Online ISSN: 2159-662X)

SNMMI SOCIETY OF NUCLEAR MEDICINE AND MOLECULAR IMAGING